AD-A081 747 VARIAN ASSOCIATES PALO ALTO CA SOLID STATE LAB F/G 17/2
III-V HETEROSTRUCTURE AVALANCHE PHOTODIODE MODULES FOR FIBER OP--ETC(U)
APR 79 R YEATS, S H CHIAO DAAB07-78-C-2402
UNCLASSIFIED NL

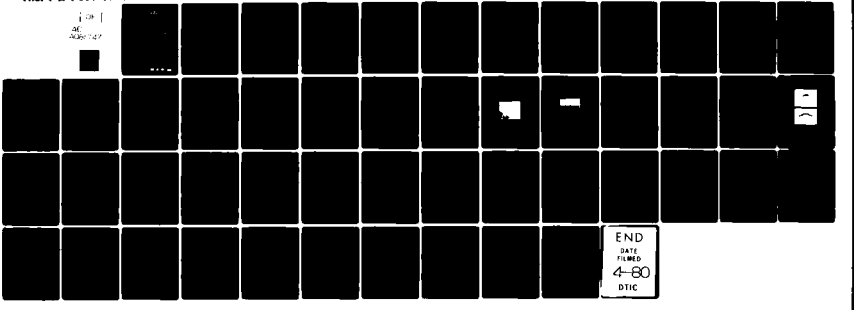

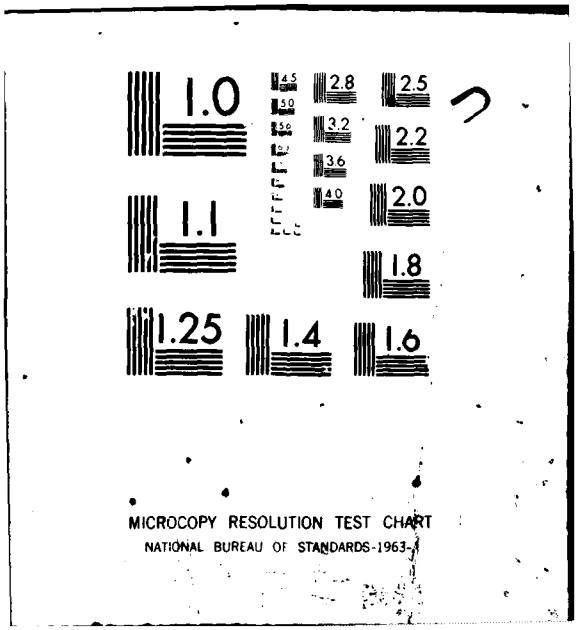
1.0
1.1
1.25
1.4
1.6
1.8
2.0
2.2
2.5
2.8
3.2
3.6
4.0
4.5
5.0
5.6
MICROCOPY RESOLUTION TEST CHART
NATIONAL BUREAU OF STANDARDS-1963-A

III-V HETEROSTRUCTURE AVALANCHE PHOTODIODE MODULES FOR FIBER OPTIC COMMUNICATION LINKS IN THE 1.0 TO 1.3 MICROMETER SPECTRAL RANGE

INTERIM REPORT NO. 2

(August 1978 - February 1979)

April 1979

Prepared for:

Department of the Army
Headquarters US Army Communications R&D Command
Fort Monmouth, NJ 07703

Contract No. DAAB07-78-C-2402

Prepared by:

R. Yeats and S. H. Chiao

Solid State Laboratory
Varian Associates, Inc.
611 Hansen Way
Palo Alto, CA 94303

UNCLASSIFIED
SECURITY CLASSIFICATION OF THIS PAGE (When Data Entered)

REPORT DOCUMENTATION PAGE		READ INSTRUCTIONS BEFORE COMPLETING FORM
1. REPORT NUMBER Interim Report No. 2	2. GOVT ACCESSION NO. -	3. RECIPIENT'S CATALOG NUMBER -
4. TITLE (and Subtitle) III-V Heterostructure Avalanche Photodiode Modules for Fiber Optic Communication Links in the 1.0 to 1.3 Micrometer Spectral Range		5. TYPE OF REPORT & PERIOD COVERED Technical Report (Aug '78--Feb. '79) 6. PERFORMING ORG. REPORT NUMBER -
7. AUTHOR(s) R. Yeats [redacted] S. H. Chiao		8. CONTRACT OR GRANT NUMBER(s) DAAB07-78-C-2402
9. PERFORMING ORGANIZATION NAME AND ADDRESS Varian Associates, Inc. 611 Hansen Way Palo Alto, CA 94303		10. PROGRAM ELEMENT, PROJECT, TASK AREA & WORK UNIT NUMBERS -
11. CONTROLLING OFFICE NAME AND ADDRESS U.S. Army Communications R&D Command Fort Monmouth, NJ 07703 (C. Loscoe)		12. REPORT DATE Apr [redacted] 79 13. NUMBER OF PAGES 30
14. MONITORING AGENCY NAME & ADDRESS (if different from Controlling Office) Interim Technical Report No. 2, Aug 78-Feb 79		15. SECURITY CLASS. (of this report) Unclassified 15a. DECLASSIFICATION/DOWNGRADING SCHEDULE
16. DISTRIBUTION STATEMENT (of this Report) DISTRIBUTION STATEMENT Approved for public release; distribution unlimited.		
17. DISTRIBUTION STATEMENT (of the abstract entered in Block 20, if different from Report)		
18. SUPPLEMENTARY NOTES		
19. KEY WORDS (Continue on reverse side if necessary and identify by block number) indium gallium arsenide phosphide photodiode indium gallium arsenide indium phosphide avalanche photodiode MICROMETERS		
20. ABSTRACT (Continue on reverse side if necessary and identify by block number) InGaAsP APDs have been fabricated with uniform high-speed gains up to 42 and quantum efficiencies up to 70% at 1.28 μm. At high gains increased leakage current leads to excessive shot noise and gain saturation. Noise measurements indicate that the increased leakage current arises from a uniformly multiplied but increasing value of the primary (i.e., premultiplication) leakage current. To try to reduce this leakage current, various procedures for fabricating → over		

DD FORM 1 JAN 73 1473 EDITION OF 1 NOV 65 IS OBSOLETE

UNCLASSIFIED 409910
SECURITY CLASSIFICATION OF THIS PAGE (When Data Entered)

20. ABSTRACT (Cont.)

guard ring APDs have been studied. Preliminary guard ring structures have demonstrated guard ring isolation by exhibiting avalanche gain in the central region only. However, these initial guard ring APDs need further development before a meaningful comparison can be made to APDs without guard rings.

SUMMARY

InGaAsP avalanche photodiodes have been fabricated with uniform high speed gains up to 42 and quantum efficiencies up to 70% at 1.28 μm. Rise and fall times have been measured down to 1 nsec or less at 1.27 μm. Leakage currents are extremely small until about 70% of the breakdown voltage. Above this point the leakage current begins to rise rapidly. The large leakage current in the avalanche gain region leads to excessive shot noise and gain saturation. Noise measurements indicate that the increased leakage current arises from a uniformly multiplied but increasing value of the primary (i.e., premultiplication) leakage current. The value of the primary leakage current thus obtained leads to a prediction of gain saturation in approximate agreement with the observed maximum gain. We have studied various procedures for fabricating guard ring APDs in an effort to reduce this leakage current. Preliminary guard ring structures have demonstrated guard ring isolation by exhibiting avalanche gain in the central region only. However, these initial guard ring APDs need further development before a meaningful comparison can be made to APDs without guard rings.

PREFACE

The work reported here was supported by the U. S. Army Communications R&D Command, Fort Monmouth, New Jersey, under Contract DAAB07-78-C-2402. The project engineer is Ms. Claire Loscoe. The program is aimed at the development of III-V high performance avalanche photodiodes for detection in the 1.0 to 1.3 micron wavelength range.

The work was carried out in the Varian Corporate Research Solid State Laboratory. Contributions to this work were made by R. Yeats, S. H. Chiao, and G. A. Antypas.

TABLE OF CONTENTS

1. INTRODUCTION

In order to take advantage of the low attenuation and low material dispersion[1] of silica fibers for wavelengths in the 1.0 to 1.3 μm region, high performance detectors must be developed for these wavelengths. Detectors operating over the range 0.9 to 1.7 μm can be fabricated from the InGaAsP materials system.[2-4] Our efforts have centered on the development of InGaAsP avalanche photodiodes (APDs) sensitive to wavelengths in the 1.0 to 1.3 μm region.

This report describes the work done in the second six-month period of research under the present contract. For a detailed account of the first six-month period, the reader is referred to the first interim report.[4]

InGaAsP avalanche photodiodes have been fabricated with uniform high speed gains up to 42 and quantum efficiencies up to 70% at 1.28 μm. Rise and fall times have been measured down to 1 nsec or less at 1.27 μm. Yields are high, about 75%, on good wafers. Across the wafer variations in breakdown voltage have had standard deviations less than 0.3 V (or 0.5%).

The only unsolved problem with these APDs is the unusually high leakage current at relatively low values of gain (e.g., 5-10). At biases up to 70% of the breakdown voltage, the leakage current is extremely low. Values as low as $1.8 \times 10^{-6} A/cm^2$ have been measured at half the breakdown voltage. Above 70% of the breakdown voltage, however, the leakage current begins to rise sharply. At high gains, the

increased leakage current leads to excessive shot noise and decreased sensitivity. Using noise measurements, we have been able to show that the leakage current is uniformly multiplied by about the same factor as the average photocurrent. Hence, the increased leakage current in the avalanche gain region is due to an increase in the premultiplication (or primary) leakage current, rather than to microplasmas. The value of the premultiplication leakage current obtained from these noise measurements leads to a prediction of gain saturation at a value approximately equal to the experimentally observed value, thus further substantiating the analysis.

To improve APD performance the primary leakage current at high biases needs to be decreased. We have seen that the leakage current is sensitive to surface treatment.[4] We have studies various procedures for fabricating guard ring APDs (GRAPDs), in an effort to reduce this leakage current. Preliminary GRAPDs have been fabricated exhibiting gain in the interior region only, as desired. However, there are still some fabrication problems that need to be solved before a significant comparison can be made between the GRAPDs and the APDs without guard rings.

One requirement of this contract was the shipment of 12 thoroughly characterized APDs. The diodes shipped represent a random sampling of devices from across a (single) wafer. Some statistical information is given later in this report, which describes the kind of variations that we are getting in a batch of APDs. In general, we found very little variation in these APDs, so that when one has seen a few APDs from a given wafer, one will know the quality of the remaining APDs from that wafer.

2. DEVICE FABRICATION

2.1 Materials Parameters

The materials InGaAsP, InGaAs, and InP have been utilized in our APD work. Layers were grown by liquid phase epitaxy (LPE) using procedures we have previously described.[4]

The InGaAsP APDs typically have room temperature bandgaps between 0.98 eV and 1.02 eV, and are typically lattice-matched to InP to within 0.003 Å or better. The active layers are n-type with a carrier concentration usually in the range 1-2 x $10^{16}cm^{-3}$ and have room temperature mobilities of about 3800 cm^2/V-sec. Breakdown voltages usually range between 50 and 90 V, but have been as high as 160 V. The conventional APD structures (i.e., those not having guard rings) have been grown on (100)-oriented Zn-doped, p-type InP substrates. The substrate carrier concentration is about 1 x $10^{18}cm^{-3}$. The Zn-doped substrates have a very low dislocation density, typically in the range 0-500/cm^2. On the other hand, the GRAPDs (guard ring APDs) have been grown on Sn-doped substrates ($n \approx 1 \times 10^{18}cm^{-3}$) and have substantially higher dislocation density ($\approx 10^4/cm^2$). Recently, some dislocation-free n-type sulfur-doped bulk InP has been grown here at Varian, and in the future is likely to be used instead of Sn-doped material for many applications.

The importance of dislocations is not yet known in the InGaAsP material system. In silicon, some dislocations are correlated with microplasmas while others have no effect whatsoever on APD performance. The importance of dislocations probably depends on what impurities are present, as only certain impurities will "dress" the dislocations.

In some of our guard ring work, InP layers are grown using standard vapor phase epitaxy (VPE) techniques,[5] rather than LPE techniques. It is difficult to grow InP on low bandgap InGaAsP layers by LPE, while it is quite easy to do so by VPE. Furthermore, the close control of carrier concentration that is required for guard ring fabrication, is more readily attained in VPE.

We have also made a substantial effort to fabricate InGaAs APDs. Our growth procedure has previously been described.[4] InGaAs has a room temperature bandgap of 0.73 eV when grown lattice-matched on InP substrates. The carrier density of the n-type layers is usually about 3-5 x $10^{16}cm^{-3}$, and the breakdown voltage is usually between 20 and 35 V.

For both the InGaAsP and InGaAs APDs, we have used primarily the (100) orientation. (100)-oriented InGaAs almost always has a room temperature lattice constant less than the lattice constant of InP. The best lattice match commonly seen has $\Delta a \approx -.005$ Å. On rare occasions exactly lattice-matched (100) InGaAs has been grown, but the surface morphology was then poor compared to InGaAs layers having lattice constants smaller than InP. The mismatch problem is probably due to the difference in thermal expansion between the $In_{.53}Ga_{.47}As$ layer and the InP substrate. $In_{.53}Ga_{.47}As$ has a thermal expansion parameter (5.66 x $10^{-6}K^{-1}$), that is about 20% larger[6] than that for InP (4.56 x $10^{-6}K^{-1}$). Hence, if a layer of $In_{.53}Ga_{.47}As$ is grown lattice matched at the growth temperature, it will be mismatched on the small side by about 0.004 Å at room temperature. In order to get lattice match at room temperature, it is necessary to grow

a layer that is mismatched at the growth temperature. However, growth under mismatched conditions results in poor nucleation and hence poor surface morphology.[7] For (100) InGaAs, the effect is strong enough that good surface morphology cannot be obtained on layers that are exactly lattice matched at room temperature. Furthermore, a mismatch of even 0.005 Å turns out to be a problem. We observed that moderately thick (5-10 μm) layers of (100) InGaAs usually develop cracks during the drive-in diffusion step, due to the thermal strain.

It is notable that (111)B-oriented InGaAs layers have much less of a nucleation problem during growth than (100) InGaAs. In fact, (111)B InGaAs layers with perfect lattice match and good surface morphology may readily be obtained at room temperature. This phenomenon suggests that in any future work on InGaAs, the (111)B orientation would be preferred.

2.2 Conventional Mesa Structure APD Fabrication

This section summarizes the fabrication procedure used in making APDs that do not have guard rings. A more detailed account has been given previously.[4]

The structure of these APDs is shown in Fig. 1. To fabricate this structure, we begin with a low dislocation density p^+-InP substrate and by LPE grow an n-type InGaAsP layer having $n \approx 1\text{-}2 \times 10^{16} cm^{-3}$ and a bandgap of about 1.00 eV. Next we grow an n-InP layer on top of this by LPE (in the same growth cycle). The InP layer is transparent to the wavelengths of interest. It has two functions: The first is to provide a convenient means of minimizing the spreading resistance. The

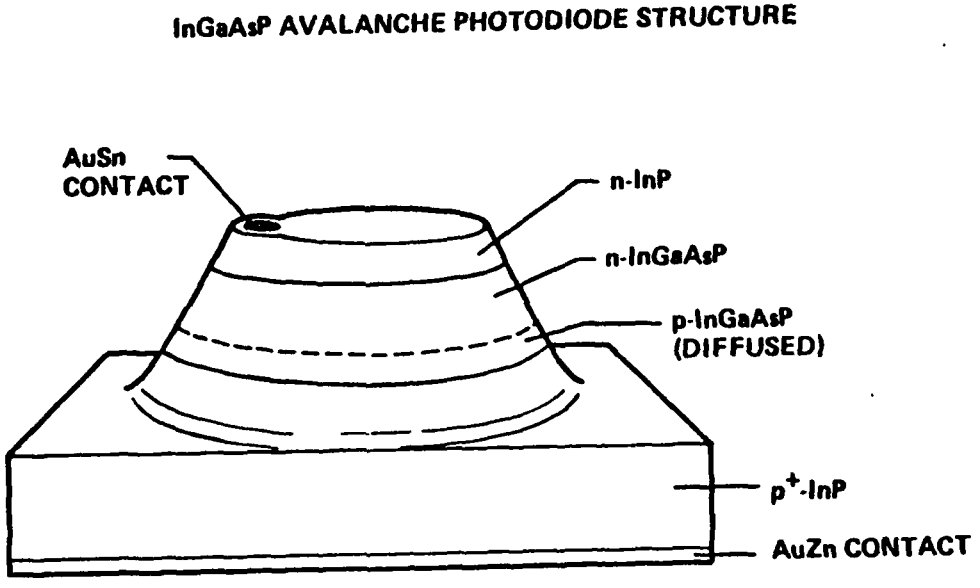

Fig. 1 InGaAsP avalanche photodiode structure.

second is to provide heterojunction confinement of carriers away from the surface, thereby increasing the quantum efficiency. Sometimes we omit this top InP layer when we are focusing on device parameters not requiring the highest quantum efficiencies.

After the epilayers are grown, their bandgaps are determined by photoluminescence, while their lattice constants are determined by X-ray diffraction. Next, the layer side of the wafer is covered with silicon nitride and is vacuum sealed into a quartz ampoule, to which a few milligrams of P have been added. The sealed ampoule is then put into a diffusion furnace to drive the p-n junction about 1 micron or more into the active layer from the substrate interface.

The ampoule is then opened and a cleaved and stained cross-section of the wafer is examined to determine the depth of the diffusion. Next, a broad-area Au-Zn metallization is evaporated and alloyed onto the p^+-InP substrate, thus forming the p-type ohmic contact. Following this, 3-mil diameter Au-Sn dots are evaporated and alloyed onto the layer side. One to two mils of Au are then electroplated onto the contacts. Next photoresist is put down on the layer side in an asymmetric "figure-8" shape, in order to define during the subsequent mesa etch the "figure-8" shaped cross-section apparent in Fig. 1. The part of the "figure-8" surrounding the Au-Sn contact has a diameter of 5-6 mils, while the other part of the "figure-8" has a diameter that varies according to the size desired for the photosensitive area. We have used diameters between 5 and 12 mils. The wafer is then etched in a solution of 2 Bromine:100 Methanol.

After the resist is removed, surface passivation is applied and the wafer is then ready for testing. While on the wafer, the diodes are typically tested for gain, breakdown voltage, leakage current, series resistance, frequency response, quantum efficiency, and capacitance. When the diodes are to be packaged, the wafer is diced up with a diamond saw and individual diodes are epoxied into high frequency packages.

There is a slight modification of these procedures when the active layer is InGaAs rather than InGaAsP. Because it is very difficult to grow InP on InGaAs by LPE, the top InP layer is grown by VPE rather than LPE.

2.3 Guard Ring APD Fabrication

2.3.1 Structure. The guard ring structure that we use is shown in Fig. 2. Here the n-type InGaAsP epilayer is grown on an n-type (Sn-doped) InP substrate. Usually the p-type regions are fabricated in a two-step diffusion process. First, a long and deep Zn diffusion is made to form the outside part (ring) of the guard ring structure. This is the curved p-InGaAsP region in Fig. 2. During this step the dopant is kept out of the interior (active) region by appropriate masking or other means. During the second step, a shallow p^+ diffusion is made to form a p-n junction in the interior region of the guard ring. Figure 2 shows a (transparent) Zn-doped p^+-InP layer as the topmost layer. This is grown on the InGaAsP layer after the first deep diffusion in order to be used as the dopant source for the (second) shallow p^+ diffusion.

Diffused guard rings work in the following way to reduce surface fields: The interior p-n junction has a breakdown voltage determined only by the level of doping in

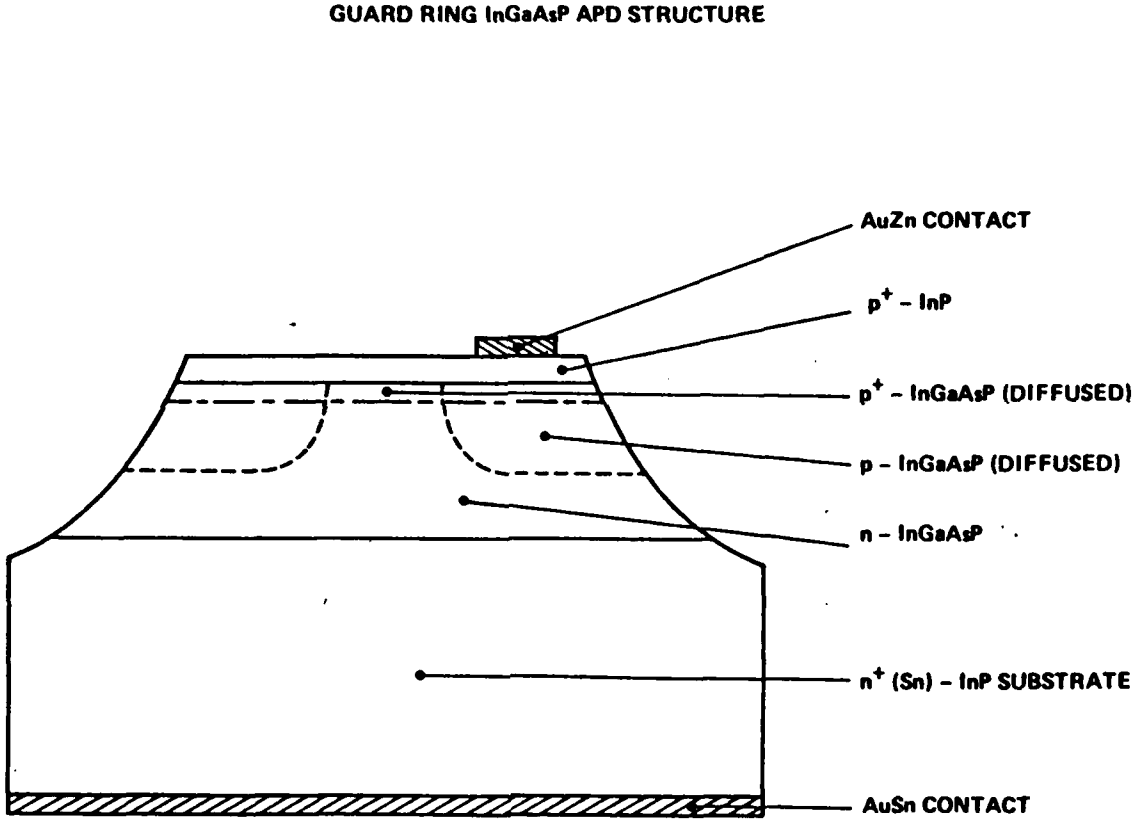

Fig. 2 Guard ring InGaAsP avalanche photodiode structure.

the n-InGaAsP active layer. This is because the p^+ side of this junction was obtained by such a shallow diffusion that the junction behaves essentially like a onesided abrupt (ungraded) junction. On the other hand, the junction formed by the ring of the guard ring is obtained from a long, deep diffusion and is graded. If the grading is flat enough the doping gradient will determine the breakdown voltage rather than the background n-level. Hence, it would be possible, for example, to have the breakdown voltage of the ring junction be twice as large as the breakdown voltage of the interior junction. This means that when the interior junction is biased into its avalanche gain region, the ring junction is at only half of its breakdown voltage. Hence, all junctions that touch the outside surface would be at only half the local breakdown voltage. The grading of the outer junction has an additional benefit. Unlike one-sided junctions, graded junctions are rather insensitive to junction curvature[8] and also to the bevel angle of the mesa.

2.3.2 Analysis of Different Guard Ring Fabrication Techniques.

A. Proton Bombardment

Guard rings formed by proton bombardment are physically different than the previously described diffused guard rings. In proton bombardment, the approach is not necessarily to make the exterior junction have a higher breakdown voltage, but rather to cause so much damage that the material becomes insulating so that no current can flow whether or not there is the potential barrier of a p-n junction. Protons are chosen rather than other ions because

they have a greater depth of penetration into the semiconductor. However, for available accelerating potentials, their range is still under 2 μm.[9] Since the width of the depletion region in our APDs is about 2 μm, it is not possible to get deep enough penetration to fully isolate the depletion region from the surfaces. To circumvent this problem, we proton bombarded diodes that had already been completely fabricated (including mesa etching). The mesa formed allowed the protons direct access to the edges of the depletion region, without having to go through an intervening layer of semiconductor.

Before the proton bombardment, the diodes consistently had breakdown voltages of about 70 V, with shunt resistances $>10^9$ ohms. After a proton dose of $10^{14}/cm^2$ at an energy of 150 keV, the diodes consistently had breakdown voltages of about 15 V with shunt resistances of about 100K ohms. We estimate the resistivity of the damaged layer to be only about 5000 ohm-cm. Apparently, the proton bombardment destroyed the built-in potential barrier to current flow of a p-n junction, without causing high enough resistivity to substantially inhibit current flow. Therefore, it does not seem likely that proton bombardment will be useful in making guard rings.

B. Ion Implantation

Guard rings formed with the aid of ion implantation differ from guard rings formed by proton bombardment in that the ions implanted are dopant atoms such as Zn. Furthermore, the damage caused during the implantation is <u>not</u> desired, and in fact is annealed away in a subsequent

step. In the fabrication of guard rings, an ion implanted region essentially serves only as a well-controlled dopant source. We are presently modifying our ion implanter for Zn and Be implantation, but have not yet fabricated any guard ring structures. Fabrication of such GRAPDs would entail two separate implantations and two separate drive-in diffusions.

C. Doped Spin-on Glasses as Diffusion Sources

These materials are available from such companies as Emulsitone. They are initially liquid in form, are spun onto the wafer like photoresist, and then oven dried. The drying removes the solvent and leaves behind an approximately 2000 Å thick layer of SiO_2 doped with a selected impurity. These spin-on glasses failed for a variety of reasons. First, it proved difficult to control the magnitude of the dopant. In spite of diluting the doped SiO_2 with undoped SiO_2 by factors as much as 100:1, the dopant level remained the same - at about solid solubility ($\sim 10^{19} cm^{-3}$). This is too high. These glasses also caused enhanced surface degradation of InP at higher temperatures (2 hours at 700°C) while not doping at all at lower temperatures (2 hours at 500°C). Overall, these doped spin-on glasses do not appear suitable for fabrication of GRAPDs.

D. Zn and Zn Alloys as Diffusion Sources

It is possible to use Zn or Zn alloys as a diffusion source. The Zn (or Zn alloy) is put into a quartz ampoule along with the wafer and a small piece of red phosphorus (to provide P overpressure). The ampoule is then vacuum sealed and put into a constant temperature furnace

for the diffusion step. To control the Zn concentration in the wafer requires the Zn vapor pressure in the ampoule to be controlled. It is extremely difficult to get a low enough vapor pressure of Zn. Diluting the Zn in In or Ga to form Zn alloys is one common technique[10] used to lower the vapor pressure of the Zn. However, we found that this only worked for large sources -- 100 mg or more. For 500 μg sources, diluting the Zn in In or Ga seemed to have no effect. Apparently equilibrium conditions only exist when the Zn alloy has a larger surface area. The problem with large sources is that they bring into the ampoule a large amount of undesired impurities. The oxides are especially troublesome because they cause enhanced surface decomposition of InP. Use of Zn or Zn alloy sources does not appear to be an attractive means for forming GRAPDs.

E. Two-Step Diffusions

We have discussed in the previous sections how it is difficult to get low Zn concentrations in InP and InGaAsP by various diffusion methods. One way to circumvent the problem is to replace a single diffusion step with two steps -- a predeposition step followed by a drive-in step. For example, one might have a predeposition step resulting in a junction 0.05 μm deep with a surface concentration at the solid solubility ($\approx 10^{19}cm^{-3}$). If this step was followed by a 5 μm deep drive-in diffusion, the surface concentration would then be about $10^{17}cm^{-3}$; i.e., reduced by about the ratio of the two junction depths. We tried this approach.

It is not practical to measure junction depths of only 0.05 μm. Such a thin p-layer diffused on an n-type layer acts like it is not there, and certainly cannot be detected

optically. What one can do is to do a very long diffusion in order to obtain a measurable junction depth. Then one can shorten the diffusion time to get any desired junction depth by knowing that the junction depth scales approximately as $\sqrt{t}$ (t = time). We tried this approach. We used a 500 μg source of 10% Zn in In in a sealed evacuated quartz ampoule. The diffusion sample was a piece of (100)-oriented n-type InP with a Sn concentration of $1 \times 10^{18} cm^{-3}$. Figure 3 shows a cleaved and stained cross-section of a sample that had been diffused into for 23.5 hours at 395°C. The junction depth is 0.8 μm. Next we diffused into a new piece of InP with the same kind of Zn source, but only for 11 minutes at 395°C. If the junction depth scales as $\sqrt{t}$, then the junction depth would now be only 0.07 μm. Not surprisingly, electrical and optical examination of this piece showed no evidence of a p-layer. Next we did a 75-minute drive-in diffusion on this piece (no Zn source present) at 850°C. A new cleaved and stained cross-section of the piece was then examined. It is shown in Fig. 4. Note there is now a junction about 3 μm deep, but that the junction depth is nonuniform. The experiment was repeated a number of times with a variety of InP wafers and always the wavy junction line resulted. For APDs, flat junctions are desired because curvature affects the local breakdown voltage. Perhaps the cause of the curvature is due to a local variation near the surface in what the level of solid solubility of Zn is. Since the predeposition depth required is only about 500 Å, the surface will have a strong influence. Surface strains or surface roughness on the scale of a few hundred angstroms could cause variations in the Zn concentration. Such variations would lead to a nonuniform junction depth following the drive-in diffusion.

Fig. 3 p-n junction location after a 23.5-hour Zn diffusion at 395°C.

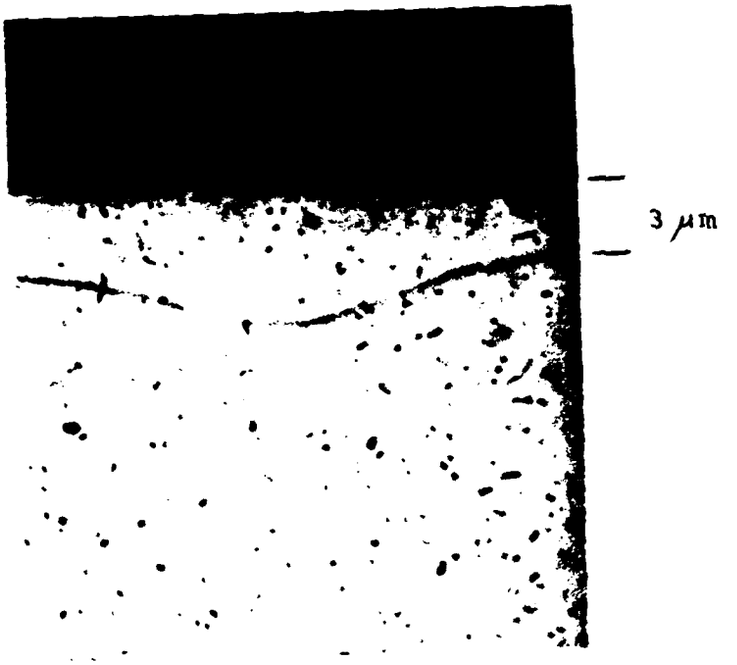

Fig. 4 p-n junction location after an 11-minute Zn diffusion at 395°C followed by a 75-minute drive-in diffusion at 850°C.

From these results we conclude that it is not practical to substantially reduce concentrations from the $10^{19}cm^{-3}$ level by using two-step diffusions.

F. InP Epilayer as a Diffusion Source

We now describe a method that, while complicated, can nevertheless be successfully used to fabricate GRAPDs. We begin with an n-type InGaAsP layer having had a layer of Zn-doped p-InP grown over it by VPE. The InP need not cover the entire surface, but may be present in any desired pattern. This can be accomplished by either oxide masking (VPE InP will not grow on SiO_2) or by selective etching through openings in photoresist using HCl (which etches InP but not InGaAsP). The p-InP can then be used as a solid source for a Zn drive-in diffusion in any desired pattern. Furthermore, the Zn concentration can be closely controlled by controlling the Zn concentration in the VPE InP epilayer--which is readily accomplished. After the drive-in diffusion is performed, the InP layer can be selectively removed with HCl, and a new layer can be grown, if desired, and an additional drive-in diffusion performed.

To obtain the structure shown in Fig. 2, two drive-in diffusions are used. The first one is a deep diffusion to form the guard ring. A p-type VPE InP layer with circular openings is used as the Zn source. After the drive-in diffusion, this layer is removed and then a new p^+-InP layer is grown over the entire surface. A shallow drive-in diffusion is then performed to obtain the final structure. The second drive-in diffusion has been included for generality, but it may not actually be necessary.

We have fabricated some preliminary GRAPDs with the above method that have had avalanche gain in the central region only, as desired. However, there are still some details of the fabrication process that need to be further developed before it is known how good GRAPDs can be compared to APDs without guard rings.

3. RESULTS AND DISCUSSION

3.1 InGaAsP Diodes without Guard Rings

InGaAsP diodes without guard rings have been fabricated that have[11] uniform high-speed gains up to 42. Figure 5 shows an InGaAsP APD operating at a gain of 40. The illumination was provided by a pulsed Varian LED emitting at 1.05 μm. The area of this diode was about $2.2 \times 10^{-4} cm^2$, (equivalent to a 6.6 mil diameter, although its shape was a "figure 8" as in Fig. 1). This diode did not have an n-InP capping layer.

The gain unformity of this diode operating at an average gain of 30 is shown in Fig. 6. The gain uniformity was determined by using the same pulsed 1.05-μm LED in combination with a corning graded index fiber that had been tapered so that a 1.5-mil spot size could be obtained for scanning the area of the APD. Scans of the entire area of this APD indicated that the local gain was within ±8% of the average gain, when the average gain was 30. At smaller gains, the uniformity is always better. At gains near 1, there is no perceptible variation in response with position. Diodes without good gain uniformity are quite rare; i.e., any diodes that pass inspection on a curve tracer are found to have uniform gain. Furthermore, most diodes on a given wafer are of comparable quality. A random sampling of diodes was made for some APDs of rather large area ($7.3 \times 10^{-4} cm^2$). (This is described further in Section 4.) We found that the across-the-wafer variations in the APDs were very small. For example, the maximum gain attainable had a standard deviation of only 20% ($M_{max} = 15.7 \pm 3.2$), while

a)

b)

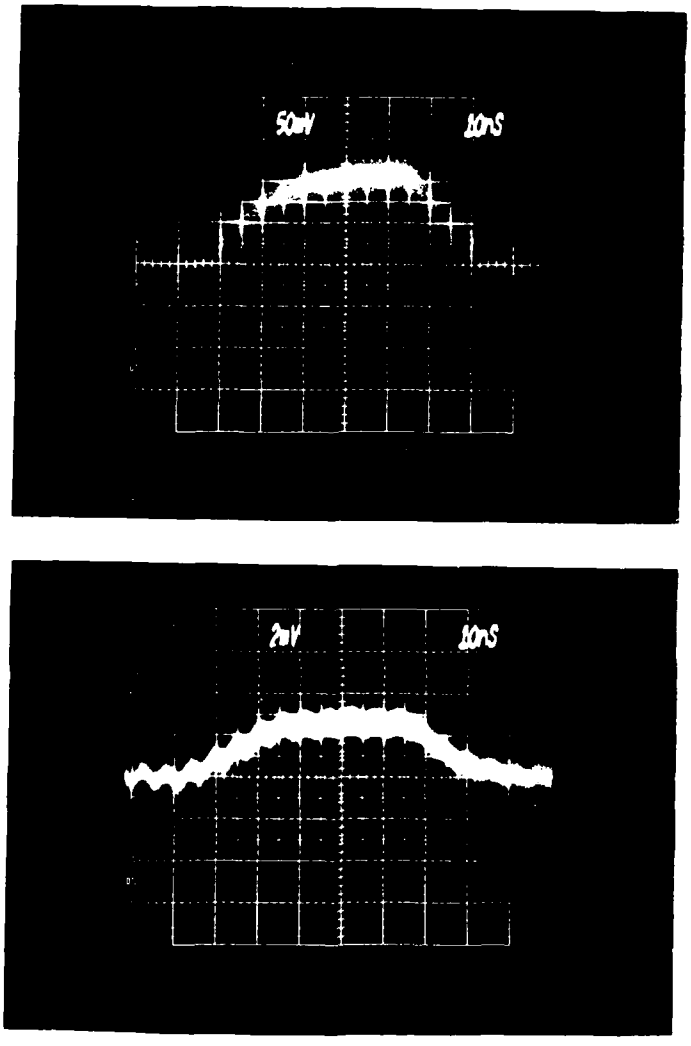

Fig. 5 InGaAsP avalanche photodiode response to a pulsed InGaAsP LED.
a) Operating at 60 V with a gain of about 40.
b) Operating at 30 V where the gain is 1.
Pulse rise and fall times are those of the LED.

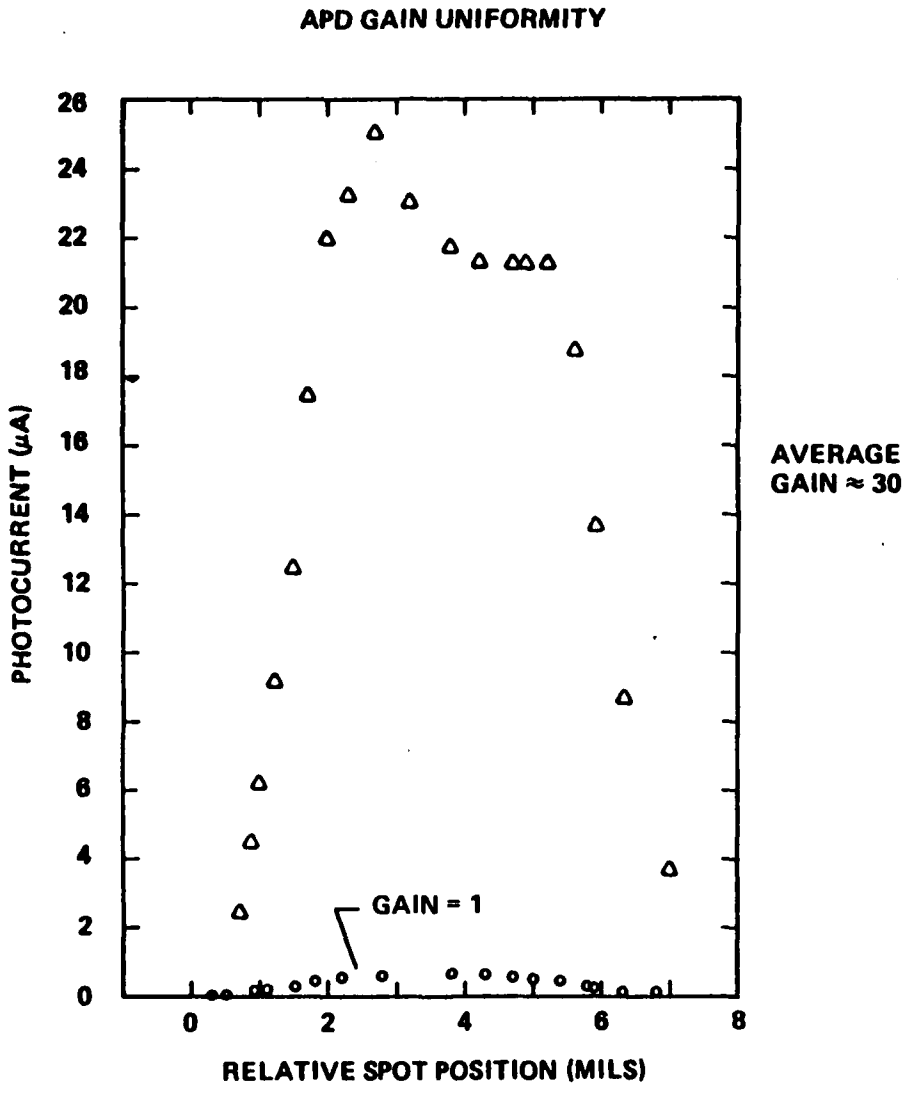

Fig. 6 Gain uniformity of an InGaAsP APD operating at an average gain of 30.

the breakdown voltage had a standard deviation of less than 0.3V (= ±0.5%). On-the-wafer yields of diodes with gains greater than 2 have been as high as 75% on good wafers. This is another strong indication of the high level of bulk uniformity attainable.

The speed of our APDs has been measured using in-house pulsed InGaAsP lasers. We use a variety of different lasers in order to get emission wavelengths throughout the range 1.1 to 1.3 μm. The laser rise and fall times are known to be less than 0.5 nsec. The speed (and quantum efficiency) of our APDs depends mainly on how close the depletion region is to the top of the (absorbing) InGaAsP layer. (See Fig. 1). This is because carriers generated by the light outside the depletion region take additional time to diffuse to the depletion region, before they contribute to the photocurrent. We have avoided placements of the p-n junction that would result in the depletion region punching through the top of the InGaAsP layer, as this is likely to increase the occurrence of premature breakdown. For 1.00 eV bandgap APDs having the edge of the depletion region 1.0 μm below the top InP layer, we measured rise and fall times ranging from 3 nsec at 1.10 μm to $\lesssim$ 1 nsec at 1.27 μm. Placing the junction a little closer to the top of the InGaAsP layer would have resulted in subnanosecond speed throughout the 1.0 to 1.3 μm range. The speed of these APDs did not vary with avalanche gain. Hence the above rise and fall times apply for operation anywhere in the avalanche gain region.

Quantum efficiencies of our APDs have been measured using in-house InGaAsP LEDs of various wavelengths. The light output is coupled to the APD through an optical fiber, tapered at one end, so that a 1.5-2.0 mil spot size can be obtained. Comparison of the APD response with the response

of a calibrated Ge detector allows the quantum efficiency to be determined. The small spot size allows the quantum efficiency to be directly measured on small area diodes. In particular, one does not have to fabricate large area diodes on the same wafer as the small area diodes in order to do quantum efficiency measurements. The LEDs used in our measurements have linewidths of about 70 meV (full width at half maximum). Measured quantum efficiencies of APDs have ranged from 63% at 1.05 μm to 71% at 1.28 μm for APDs with no anti-reflection coating. This compares to a theoretical maximum value of about 70%. The largest quantum efficiencies have been obtained in APDs having an InP capping layer on top of the quaternary layer, as in Fig. 1. Presumably this is because of the resulting heterojunction confinement. To obtain maximum quantum efficiency, especially at the shorter wavelengths where the absorption coefficients are greatest, requires that the depletion region be close to the top of the InGaAsP absorbing layer. For 1.24 μm bandgap APDs having the edge of the depletion region 1.0 μm below the top InP layer (Fig. 1), we found typical quantum efficiencies of 26% at 1.06 μm, 55% at 1.21 μm, and 63% at 1.28 μm. The quantum efficiency at 1.28 μm is higher than one might expect for a 1.24 μm bandgap quaternary. This is partly due to the absorption edge being somewhat extended in p-type material[2], and partly due to the finite linewidth of the LEDs.

We have also measured the temperature dependence of the breakdown voltage of our APDs. For APDs with a breakdown voltage of about 60V, we found

$$\Delta|V_{BD}|/\Delta T = -15 \text{ mV/°C} \quad , \qquad (1)$$

if the breakdown voltage, V_{BD}, is defined at constant current (50 μA). On the other hand, when we defined V_{BD} at constant gain (M = 2), we found

$$\Delta|V_{BD}|/\Delta T = +20 \text{ mV/°C} \quad . \tag{2}$$

The temperature range used was between room temperature and about 80°C. Note that Eqs. (1) and (2) have the opposite sign. Equation (2) is similar to the results for silicon APDs. The result in Eq. (1) occurs because the leakage current varies with temperature faster than the gain.

The leakage current in our APDs is the main cause of limited device performance. We now begin an extended discussion of leakage current and its effects.

The leakage current for a good 7-mil diameter InGaAsP APD is below 1nA at low biases, rises to 5 nA at 70% of the breakdown, and shortly thereafter increases very rapidly. At half the breakdown voltage, the leakage current is still extremely small. We have measured current densities there as small as $1.8 \times 10^{-6} A/cm^2$ (e.g., 1.3 nA/$7.3 \times 10^{-4} cm^2$). Unfortunately, as the breakdown voltage is approached, the leakage current increases rapidly. This is illustrated in Fig. 7 which shows the gain, M, as a function of leakage current for the diode of Fig. 5. The large leakage current in the avalanche gain region causes excess noise, and as we shall see, also causes gain saturation. The value of the equivalent APD noise current I_n as a function of leakage current, I_D, is shown in Fig. 8 for the diode of Fig. 5. Measurements were made by amplifying the output of the APD with a broadband 80-MHz amplifier system and feeding the resultant signal into a power meter. Knowing the amplifier characteristics (which were checked with a calibrated signal

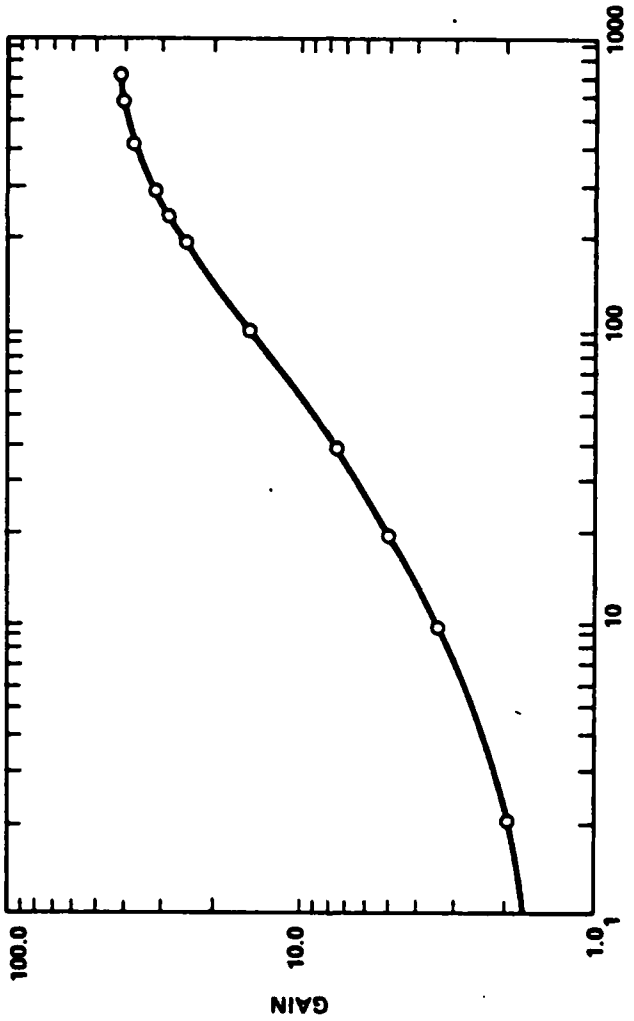

Fig. 7 Dependence of gain on leakage current for an InGaAsP APD.

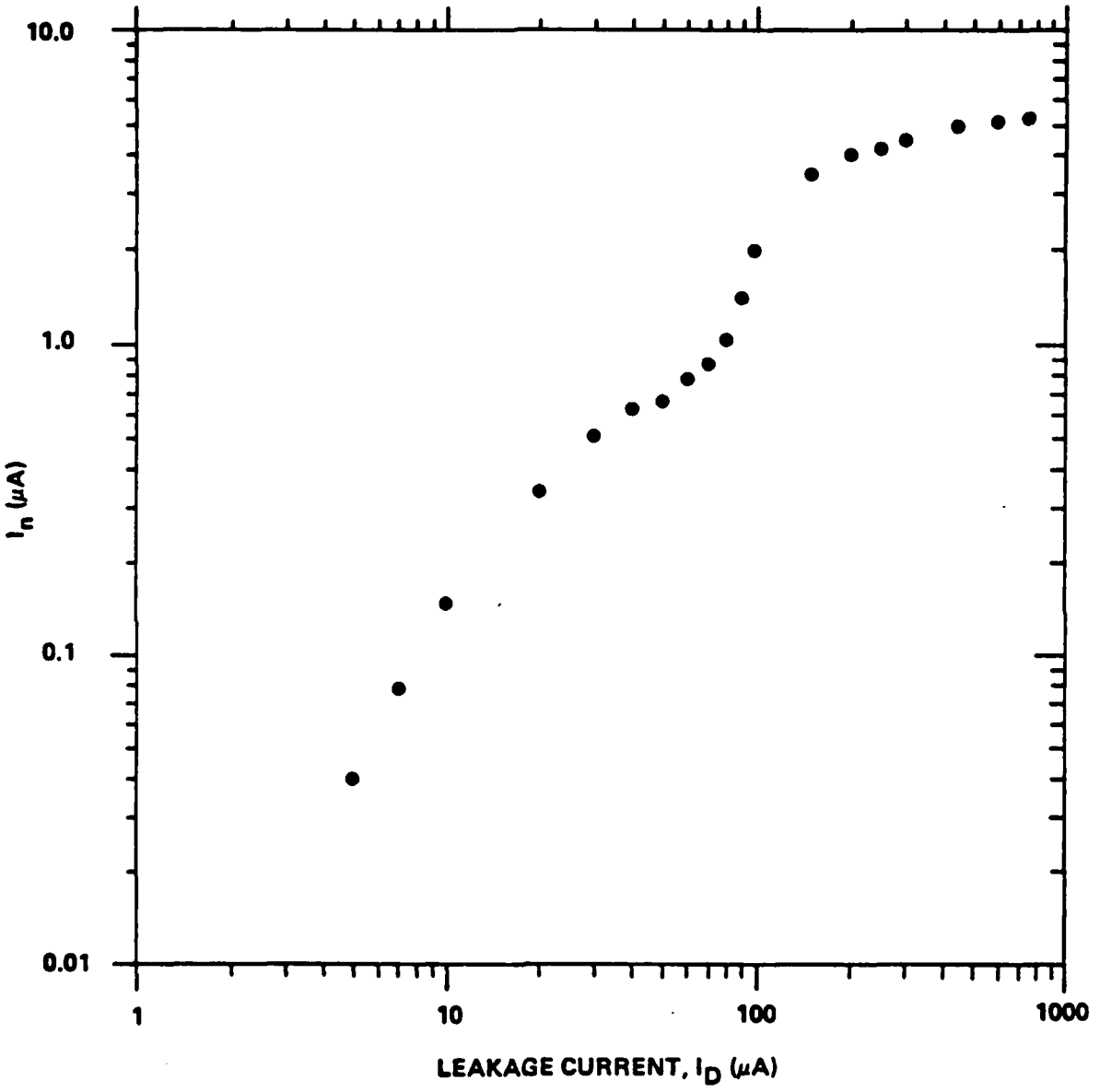

Fig. 8 APD noise current versus leakage current in an 80-MHz bandwidth.

generator), the measured noise power can be referred to the output of the APD and described as a noise current. Figures 7 and 8 show that to get a gain of 40 requires about 500 μA of leakage current and results in a broadband (80 MHz) noise current of 5 μA. Good high sensitivity 80-MHz transimpedance preamps have an equivalent input noise current of about 0.04 μA. The APD noise current equals this value at a gain of just over 2. Hence, although a gain of 40 is available, a gain of 2 would be optimum. Wider bandwidths and noisier amplifiers would result in a somewhat higher value of the optimum gain.

A clue to the nature of the leakage current can be obtained by analysis of the noise results. The APD noise current is expected to be given by[12]

$$I_n^2 = 2eBI_oM^2F = 2eBI_DMF \quad . \tag{3}$$

Here, B is the noise bandwidth, M is the current gain, and F is the excess noise factor, which itself is a function of gain. I_o is the dc component of the current to be multiplied (its premultiplication value). We wish to apply Eq. (3) to the leakage current, assuming it is multiplied, so on the right hand side of Eq. (3) we have expressed the noise current in terms of the directly measured value of the dc leakage current, I_D (= MI_o).

Using Eq. (3) we can associate a value of gain with the leakage current if we know what F is. If electron and hole ionization coefficients were equal, then F = M. If they were unequal, then $F \approx M^s$, where s is greater than or less than unity, depending on which carriers initiated the avalanche.[12] For avalanche multiplication of the leakage

current, the avalanching will be initiated by a mixture of electrons and holes. This nonpure initiation will tend to move the value of s towards s = 1, the same value of s as for equal ionization coefficients. Hence, a reasonable first approximation for F is to assume F ≈ M. Let us call M^* the resulting gain associated with the leakage current and derived from Eq. (3) under the assumption F = M. Then,

$$M^* = I_n(2eBI_D)^{-1/2} \quad . \tag{4}$$

Figure 9 shows M^* as a function of I_D for the diode of Fig. 5. The actual photocurrent gain, M, is also plotted. Note that $M^* \sim M$ with $M^* \approx 2M$ at lower values of M and with $M^* \lesssim M$ at higher values. Similar data was obtained for another diode[13] (with a modified amplifier system) and is shown in Fig. 10. For this diode, we found $M^* \lesssim M$ at all values of M. Values of $M^* >> M$ would indicate severe gain nonuniformity, while values of $M^* << M$ would indicate shunt leakage around the p-n junction. The approximations, previously described in leading to the definition of M^*, allow us to expect only roughly that M^* should be equal to M, even for an ideal diode. The observed result that $M^* \sim M$ makes it unlikely that there is either large gain nonuniformity or large shunt leakage. If $M^* \approx M$, then the rapid rise in leakage current in the avalanche gain region is <u>not</u> due to hidden gain nonuniformity, but instead is due to a rise in the premultiplication leakage current.

We now show how the increase in leakage current is the cause of gain saturation. Our noise measurements have shown that the leakage current and photocurrent have about the same multiplication. With this assumption, we can extend

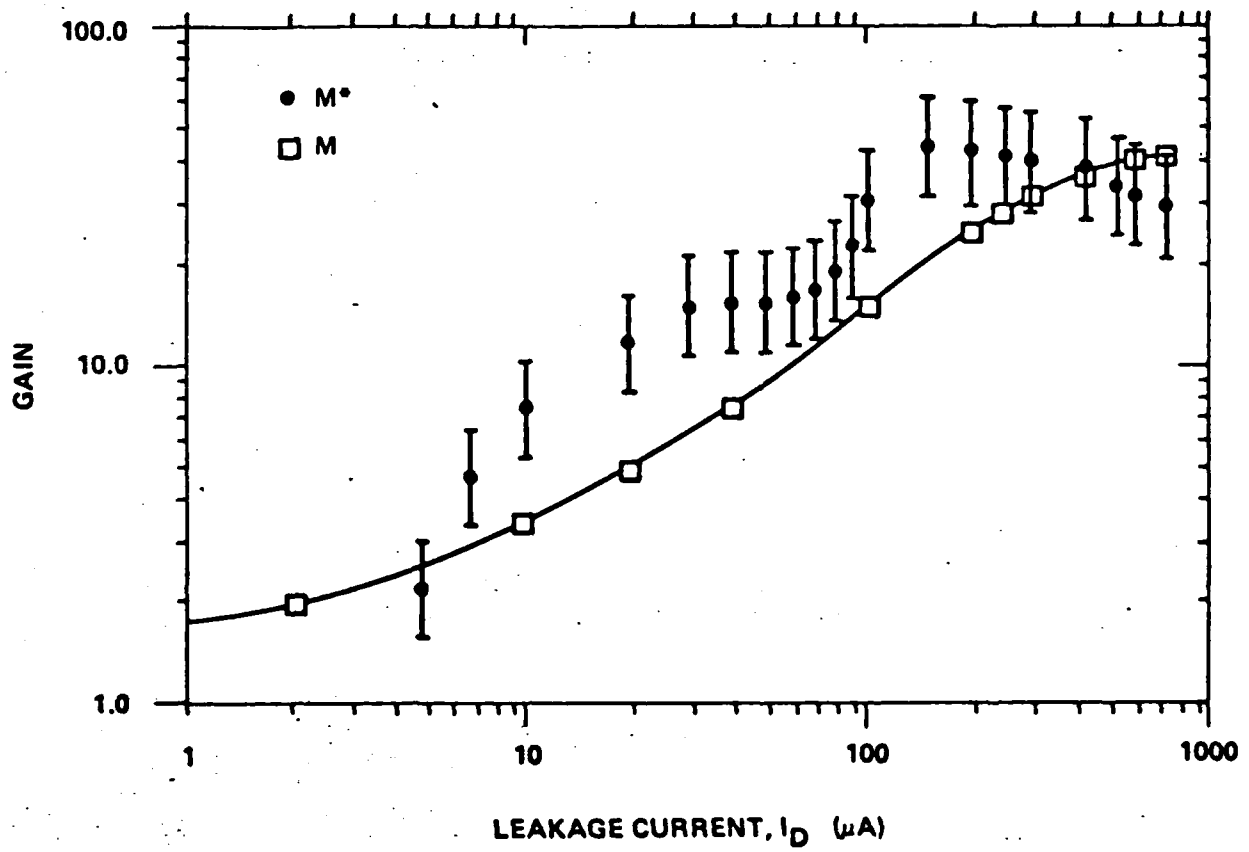

Fig. 9 APD leakage current (M*) and photocurrent (M) gain comparison.

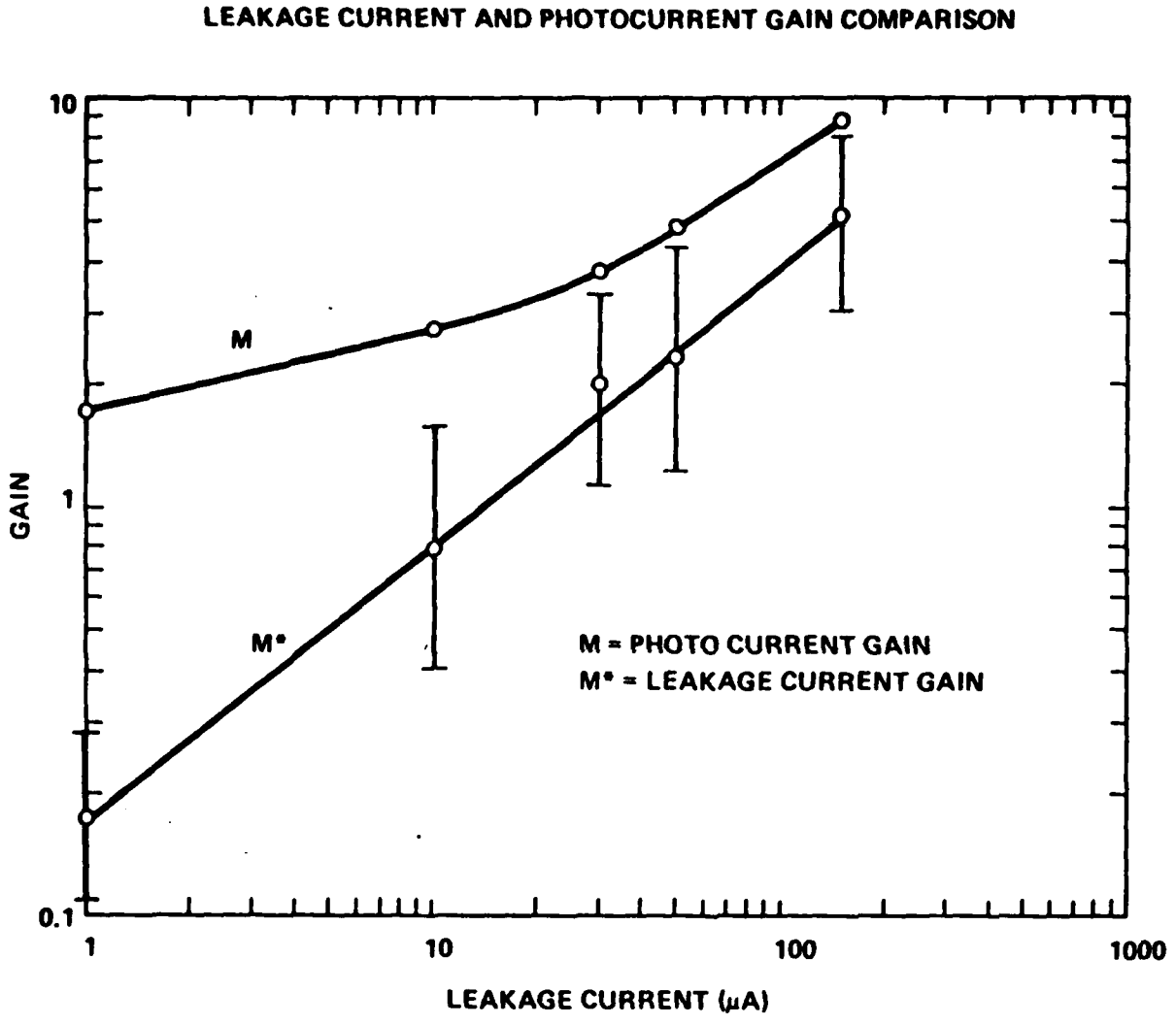

Fig. 10 APD leakage current (M*) and photocurrent (M) gain comparison.

the analysis of McIntyre[14] to primary photocurrents of any size to show that the maximum gain is

$$M_{max} = (V_B/nI_pR)^{1/2} \left[1 + (I_o/I_p)^{1/2}\right]^{-1} \quad . \tag{5}$$

Here, I_o is the premultiplication leakage current and I_p is the sum of I_o and the primary photocurrent. V_B is the breakdown voltage, R is the total[14] series resistance in the avalanche region and n is a constant obtained from the observed dependence of M on voltage[14] at small values of M.

McIntyre's well-known result

$$M_{max} = (V_B/nI_pR)^{1/2} \tag{6}$$

is generally valid only at large photocurrents and overestimates the maximum gain by a factor of two if extrapolated to small photocurrents.

For the diode of Fig. 5, we have found V_B = 57.6V, n = 4.8 ± 0.3, and R = 150Ω. (R was obtained at a reverse current of 20 mA where the I-V was quite linear, as required.) Figure 7 shows that the maximum gain occurs near $I_p \approx 800$ μA where $M \approx 42$. Our noise measurements indicate that the leakage current is multiplied by about the bulk gain. Hence, we estimate $I_o \approx 800$ μA/42 = 19 μA. Equation (5) then shows that the maximum gain occurs at small photocurrents, and has a value of $M_{max} = 32$, which is in rather good agreement, considering the various assumptions, with the observed maximum broad-area gain of about 42. Hence, both the gain saturation and noise performance are well explained simply by an increase in the value of the premultiplication leakage current.

Every method of measuring gain uniformity has indicated that the gain is indeed uniform. It now seems pretty clear that the problem with the leakage current arises from an increase in the premultiplication leakage current. As the breakdown voltage is approached, excess carriers are being generated and then multiplied by the bulk gain.

It may be that the surfaces are the cause of the excess carrier generation, and hence we have been studying fabrication of guard ring structures. The leakage current has shown considerable sensitivity to surface treatment[4] and in some cases even to the nature of the ambient gas[4]; e.g., some APDs have decreased leakage current when SF_6 is used instead of air. It is also possible that the surfaces have an inversion layer. Such a surface p-n junction could have a slightly lower breakdown voltage then the bulk, but due to the large series resistance of a thin layer, might not exhibit enhanced photocurrent gain. The effect would be that the leakage current would begin to increase at lower voltages than the gain does--which is exactly the problem our APDs have.

3.2 Guard Ring InGaAsP Diodes

We have discussed various GRAPD fabrication techniques in Section 2.3. The technique that has proved most successful to date has been the use of Zn-doped VPE InP layers as sources for selective Zn diffusion. Our results so far are very preliminary--only one wafer has been taken through the complete fabrication process, and there were still a number of problems present. Hence we do not yet have an appreciation for how good guard ring APDs can be. However, we do have a demonstration of the feasibility of guard ring fabrication.

Uniformity scans of the GRAPDs showed that they exhibited avalanche gain only in the central region of the devices--as desired. On the same wafer with the GRAPD diodes, we fabricated ordinary APDs that had only the ring junction present (i.e., the junction formed by the deep diffusion). We found that these ring junction diodes also exhibited avalanche gain and had a breakdown voltage (85V) that was 35V higher than the GRAPD diodes. Hence we have demonstrated guard ring isolation in InGaAsP.

There were some substantial problems in the fabrication of the above GRAPDs, and so we do not yet know whether a good GRAPD outperforms a good APD that does not have a guard ring. The fabrication problems now present are not fundamental ones. We expect that we will soon have good GRAPDs, thus allowing a meaningful comparison to APDs without guard rings.

3.3 InGaAs Diodes

We have made a substantial effort to make InGaAs APDs, lattice matched to InP. Our efforts have largely been on the (100) orientation. The basic structure consists[4] of an n-type InGaAs layer grown on a p^+-InP substrate. A drive-in diffusion is performed resulting in an InGaAs homojunction. We have had wafers with consistent apparent breakdown voltages of ~ 35V, low leakage (~5nA) until about 2/3 of the apparent breakdown voltage, but have never seen

any true avalanche gain. Once, on one diode, we thought we had seen gain, but it turned out to be a surface charging effect. We feel that we have made (100)-oriented InGaAs APD structures of very high quality, and yet have not seen gain. Hence we feel that fundamental changes will be required before true avalanche multiplication will be seen in (100) InGaAs. Curve-tracer gain for InGaAs diodes (lattice matched to InP) has been reported[15]; however, there is a conspicuous absence of any demonstration of rf gain. We have previously reported[4] that it is possible to get low-frequency gains up to 200 in InGaAsP APDs by special surface treatments. Such gains are reduced to less than one, however, for pulses narrower than about 100 μsec.

The problem with InGaAs diodes might be simply that the lower bandgap results in much larger leakage currents. As we have seen, leakage current limits the maximum gain attainable. InGaAs has a bandgap approximately 0.27 eV lower than a 1.00 eV quaternary. Hence, leakage currents could be increased by a factor as large as $\exp(\Delta E_g/kT) = 5 \times 10^4$. Equation 5 shows that even an increase by a factor of 100 would reduce the maximum gain attainable by a factor of 10. Hence a maximum gain of 10 in a 1.00 eV bandgap diode would become a maximum gain of 1.0 in a lower bandgap diode with 100 times more leakage current, but which was otherwise identical. If the leakage current turns out to be a surface problem, then guard rings might be all that is needed to make good InGaAs APDs. However, we are not now attempting to make new InGaAs APDs of any type.

4. SUMMARY OF DATA AND STATISTICAL INFORMATION ON A GROUP OF APDs

As part of this contract work, Varian delivered 12 well-characterized APDs to the U.S. Army Electronics Command at Fort Monmouth for testing. This provided us with an opportunity to ascertain what variations occur between APDs from different parts of the same wafer. The APDs had the structure of Fig. 1, and had a total area of $7.3 \times 10^{-4} cm^2$. We found that there was little variation between APDs, so that the APDs delivered were not preselected. The only preselection done was to eliminate diodes with obvious premature breakdowns; i.e., those that broke down at low voltages or which had kinks in their I-V characteristics. (This is the kind of preselection that would be done before even attempting to package the chips.) Hence the 12 APDs delivered represent an approximately random sampling of APDs from the wafer.

We found that the breakdown voltages were extremely constant. When the breakdown voltage is defined as the voltage where the leakage current is 10 μA, we found

$$V_{BD} \ (I_D = 10 \ \mu A) = 62.3 \pm .3V$$
$$= 62.3V \pm 0.5\%$$

while the gain at this leakage current was

$$M(I_D = 10 \ \mu A) = 2.61 \pm .08$$
$$= 2.61 \pm 3\% \ .$$

If the measurements are done at 50 μA of leakage current, one finds

$$V_{BD}(I_D = 50\ \mu A) = 65.9 \pm .3V$$
$$= 65.9V \pm 0.5\%$$

and

$$M(I_D = 50\ \mu A) = 4.82 \pm .15$$
$$= 4.82 \pm 3\% \quad .$$

The ± values given here and below are calculated standard deviations. Gains were measured by observing a 1 MHz sine wave signal on an oscilloscope. The known measurement accuracy possible was about ± .1V for V_{BD} and ± 3% for M. Hence the gain at a given leakage current has no significant variation across the wafer and the breakdown voltage varies by less than 1/2 of one percent. The uniformity is striking.

We also measured the maximum broad area gain obtainable from each of these diodes and found

$$M_{max} = 15.7 \pm 3.2 \quad .$$

The values of M_{max} ranged between 11.0 and 20.6. Gains of 20 occurred at about 500 μA of leakage current. These are fairly large area diodes, so the maximum gain is substantially less than the maximum gain of 42 measured on a smaller area diode (Section 3.1). The larger area will be required for efficient coupling to optical fibers if the diodes are to be mounted in a hermetic package.

We measured the gain uniformity at 1 MHz on each of the 12 delivered diodes using a 2-mil spot size of 1.065 μm light, obtained from an LED sinusoidally modulated at 1.0 MHz. For each diode the quantity

$$\frac{\Delta M}{\bar{M}} = \frac{M_{max} - M_{min}}{\frac{1}{2}(M_{max} + M_{min})}$$

was calculated, for average gains $\bar{M}$ of about 10. Here M_{max} and M_{min} refers to the local gain extremes. For the 12 APDs, we found

$$\frac{\Delta M}{\bar{M}} = .099 \pm .048 \quad .$$

The rise and fall times had more substantial variations. In the avalanche gain region, we found, for 1.10 μm radiation,

$$\text{rise-time} = 3.4 \pm 1.0 \text{ nsec}$$
$$\text{fall-time} = 3.6 \pm 2.2 \text{ nsec.}$$

Rise and fall times at zero bias varied between 5 and 10 nsec, but complete data was not gathered. The speed was substantially faster for longer wavelengths.

For the quantum efficiencies, η, at different wavelengths, we found

$$\eta(1.065 \text{ μm}) = (26.4 \pm 2.0)\%$$
$$\eta(1.210 \text{ μm}) = (54.6 \pm 3.2)\%$$
$$\eta(1.278 \text{ μm}) = (62.8 \pm 6.3)\% \quad .$$

The quantum efficiency at the shortest wavelength could have been improved by locating the depletion region closer to the top of the InGaAsP layer, as discussed in Section 3.1. For these diodes, the edge of the depletion region was about 1.0 μm below the top of the InGaAsP layer.

Finally, we determined the temperature coefficient of breakdown voltage to be -14.9 ± 2.4 mV/°C. Here the breakdown voltage, V_{BD}, was defined at constant current (50 μA). When we defined V_{BD} at constant gain (M = 2), we found for the one diode measured, the coefficient +25 meV/°C. This subject has been further discussed in Section 3.1.

5. FUTURE PLANS

In the future we plan on concluding our guard ring work. We wish to make guard rings that have no known problems, so that we may compare good guard ring APDs to APDs without guard rings. If they turn out to have similar leakage current in the avalanche gain region, then we would know that the leakage current is a bulk problem rather than a surface problem. Hopefully this will not be the case, but if it is a bulk problem, then more fundamental materials studies will be required before any major improvements are likely to be made in these APDs.

We are also beginning the design and fabrication of an APD/preamp module. Soon this will become the largest part of our research effort under this contract.

6. REFERENCES

1. J. Conradi, F. P. Kapron, J. C. Dyment, IEEE Trans. Electron Devices ED-25, 180 (1978).

2. H. H. Wieder, A. R. Clawson, and G. E. McWilliams, Appl. Phys. Lett. 31, 468 (1977).

3. J. J. Hsieh, J. Electron. Mater. 7, 31 (1978).

4. R. Yeats, S. H. Chiao, Interim Report No. 1, "III-V Heterostructure Avalanche Photodiode Modules for Fiber Optic Communication Links in the 1.0 to 1.3 Micrometer Spectral Range," U.S. Army Electronics Command Contract No. DAABO7-78-C-2402, September (1978).

5. R. D. Fairman, M. Omori, F. B. Fank, in 1976 Proc. 6th Int. Symp. on Gallium Arsenide and Related Compounds, (Inst. Phys. Conf. Ser. 33b) p. 45.

6. R. Bisaro, P. Merenda, T. P. Pearsall, Appl. Phys. Lett. 34, 100 (1979).

7. M. Feng, M. M. Tashima, R. H. Windhorn, G. E. Stillman, Appl. Phys. Lett. 33, 533 (1978).

8. S. M. Sze, Physics of Semiconductor Devices (Wiley-Interscience, New York, 1969), pp. 122 ff.

9. J. F. Gibbons, W. S. Johnson, S. W. Mylroie, Projected Range Statistics, Semiconductor and Related Materials, second edition (Dowden, Hutchinson & Ross, Inc., Stroudsburg, PA, 1975).

10. E. A. Rezek, P. D. Wright, N. Holonyak, Jr., Solid-State Electron. 21, 325 (1978).

11. R. Yeats, S. H. Chiao, Appl. Phys. Lett. 34, 583 (1979).

12. R. J. McIntyre, IEEE Trans. Electron. Devices ED-13, 164 (1966).

13. Diode #11 of the diodes described in Sec. 4.

14. R. J. McIntyre, IEEE Trans. Electron. Devices ED-13, 829 (1966).

15. T. P. Pearsall, M. Papuchon, Appl. Phys. Lett. 33, 640 (1978).

DISTRIBUTION LIST

Defense Documentation Center
ATTN: DDC-TCA
Cameron Station (Bldg 5)
12 Alexandria, VA 22314

Director
National Security Agency
ATTN: TDL
1 Fort George G. Meade, MD 20755

DCA Defense Comm Engrg Ctr
Code R123, Tech Library
1860 Wiehle Ave
1 Reston, VA 22090

Defense Communications Agency
Technical Library Center
Code 205 (P. A. Tolovi)
1 Wash, DC 20305

Office of Naval Research
Code 427
1 Arlington, VA 22217

GIDEP Engineering & Support Dept
TE Section
P O Box 398
1 Norco, CA 91760

Director
Naval Research Laboratory
ATTN: Code 2627
1 Wash, DC 20375

Commander
Naval Electronics Laboratory Ctr
ATTN: Library
1 San Diego, CA 92152

Cdr, Naval Surface Weapons Ctr
White Oak Laboratory
ATTN: Library, Code WX-21
1 Silver Spring, MD 20910

Commandant, Marine Corps
HQ, US Marine Corps
ATTN: Code LMC
1 Wash, DC 20380

HQ, US Marine Corps
ATTN: Code INTS
1 Wash, DC 20380

Command, Control & Communications Div
Development Center
Marine Corps Development & Educ Cdmd
1 Quantico, VA 22134

Naval Telecommunications Command
Technical Library Code 91L
4401 Massachusetts Avenue, NW
1 Wash, DC 20390

Naval Air Systems Command
Code: AIR-5332
2 Wash, DC 20360

AUL/LSE 64-285
1 Maxwell, AFB, AL 36112

Rome Air Development Center
ATTN: Documents Library (TILD)
1 Griffiss AFB, NY 13441

Air Force Geophysics Lab
L. G. Hanscom AFB
ATTN: Lib
1 Bedford, MA 01730

HQ ESD (DRI)
L.G. Hanscom AFB
1 Bedford, MA 01731

HQ, AFCS
ATTN: EPECRW Mail Stop 1058
1 Richards-Gebaur AFB, MO 64030

HQ, Air Force Electronic Warefare Ctr
ATTN: SURP
1 San Antonio, TX 78243

HQ, Air Force Systems Command
ATTN: DLCA
Andrews AFB
1 Wash, DC 20331

DISTRIBUTION LIST

Cdr, MIRADCOM
Redstone Scientific Info Center
ATTN: Chief, Document Section
2 Redstone Arsenal, AL 35809

Commander
US Army Intelligence Center
& School
ATTN: ATSI-CD-MD
1 Fort Huachuca, AZ 85613

Commander
HQ Fort Huachuca
ATTN: Technical Reference Div
1 Fort Huachuca, AZ 85613

Commander
USASA Test & Evaluation Center
ATTN: IAD-CDR-T
1 Fort Huachuca, AZ 85613

Dir, US Army Air Mobility R&D Lab
ATTN: T. Gossett, Bldg 207-5
NASA Ames Research Center
1 Moffett field, CA 94035

HQDA (DAMO-TCE)
1 Wash, DC 20310

Deputy for Science & Technology
Office, Assist Sec Army (R&D)
1 Wash, DC 20310

HQDA (DAMA-ARP/Dr. F. D. Verderame)
1 Wash, DC 20310

Cdr, Harry Diamond Laboratories
ATTN: Library
2800 Powder Mill Road
1 Adelphi, MD 20783

Director
US Army Ballistic Research Labs
ATTN: DRXBR-LB
1 Aberdeen Proving Ground, MD 21005

Director
US Army Ballistic Research Labs
ATTN: DRXBR-CA (Dr. L. Vandekieft)
1 Aberdeen Proving Ground, MD 21005

Director
US Army Materiel Systems Analysis Acty
ATTN: DRXSY-T
1 Aberdeen Proving Ground, MD 21005

Cdr, AVRADCOM
ATTN: DRSAV-E
P O Box 209
1 St Louis, MO 63166

Commander
Picatinny Arsenal
ATTN: SARPA-ND-A-4 (Bldg 95)
1 Dover, NJ 07801

Director
Joint Comm Office (TRI-TAC)
ATTN: TT-AD (Tech Docu Cen)
1 Fort Monmouth, NJ 07703

Project Manager, REMBASS
ATTN: DRCPM-RBS
2 Fort Monmouth, NJ 07703

Project Manager, NAVCON
ATTN: DRCPM-NC-TM
Bldg 2539
1 Fort Monmouth, NJ 07703

Commander
US Army Satellite Communications Agcy
ATTN: DRCPM-SC-3
1 Fort Monmouth, NJ 07703

Cdr,US Army Research Office
ATTN: DRXRO-IP
P O Box 12211
1 Research Triangle Park, NC 27709

Cdr, US Army Tropic Test Center
ATTN: STETC-MO-A (Tech Library)
Drawer 942
1 Fort Clayton, Canal Zone 09827

Commander, DARCOM
ATTN: DRCDE
5001 Eisenhower Ave
1 Alexandria, VA 22333

Cdr, US Army Signals Warfare Lab
ATTN: DELSW-OS
Arlington Hall Station
1 Arlington, VA 22212

DISTRIBUTION LIST

Commander
US Army Training & Doctrine Command
ATTN: ATCD-TEC
1 Fort Monroe, VA 23651

Director, Night Vision Laboratory
US Army Electronics R&D Command
ATTN: DELNV
1 Fort Belvoir, VA 22060

Commander
US Army ERADCOM
NV/EO Lab ATTN: Dr. R. G. Buser
1 Fort Belvoir, VA 22060

Cdr/Dir Atmospheric Sciences Laboratory
US Army Electronics Command
ATTN: DRSEL-BL-SY-S
1 White Sands Missile Range, NM 88002

Chief, Avaiation Electronics Div (SIMO)
US Army Electronics Command
ATTN: DRSEL-SI-AE, P O Box 209
1 St Louis, MO 63166

Chief
Intel Material Dev & Support Ofc
Electronic Warfare Lab, ECOM
1 Fort Meade, MD 20755

Hanscom AFB
ATTN: Dr. Eirug Davies (ESO)
Deputy for Electronic Technology
1 Bedford, MA 01730

MIT - Lincoln Laboratory
ATTN: Library (RM A-082)
P O Box 73
2 Lexington, MA 02173

NASA Scientific & Tech Info Facility
P O Box 8757
Baltimore/Washington Intl Airport
1 Baltimore, MD 21240

Advisory Group on
Electron Devices
201 Varick Street, 9th Floor
2 New York, New York 10014

Advisory Group on
Electron Devices
ATTN: Secy, Working Group D (Lasers)
201 Varick Street
2 New York, NY 10014

TACTEC
Battelle Memorial Institute
505 King Avenue
1 Columbus, OH 43201

Ketron, Inc.
ATTN: Mr. Frederick Leuppert
1400 Wilson Blvd Architect Bldg
1 Arlington, VA 22209

R. C. Hansen, Inc.
P O Box 215
1 Tarzana, CA 91356

Wright Patterson Air Force Base
ATTN: Dr. D. J. Peacock
1 AFAL/DHO, Ohio 46433

Naval Ocean Systems Center
ATTN: Dr. W. Putnam
Code 8115
1 San Diego, CA 92152

Naval Ocean Systems Center
ATTN: Dr. Steve Miller
Code 922
1 San Diego, CA 92152

Laser Diode Labs
ATTN: Dr. R. Gill
205 Forrest Street
1 Metuchen, NJ 08840

Rockwell International Science Center
ATTN: Dr. L. Tomasetta
1049 Camino Dos Rios
Post Office Box 1085
1 Thousand Oaks, CA 91360

Bell Telephone Laboratory
ATTN: Dr. R. Nahory
1 Holmdel, NJ 07733

DISTRIBUTION LIST

RCA Laboratories
ATTN: Dr. C. Neuse
David Sarnoff Research Laboratories
1 Princeton, NJ 08540

University of Illinois at
Urbana-Champaign
ATTN: Dr. G. E. Stillman
Department of Electrical Engineering
1 Urbana, IL 61801

RCA Limited
ATTN: Dr. R. J. McIntyre
Trans Canada Highway
1 Ste Anne-de-Bellevue, Quebec, Canada
H9X3L3

RCA Limited
ATTN: Dr. P. Webb
Trans Canada Highway
1 Ste Anne-de-Bellevue, Quebec, Canada
H9X3L3

MIT Lincoln Laboratory
ATTN: Dr. C. Hurwitz
P. O. Box 73
1 Lexington, MA 02173

Bell-Northern Research
ATTN: Mr. Barrie Kirk
10652 Wayridge Drive
1 Gaithersburg, MD 20760

ITT-Electro-Optical Div
ATTN: Dr. A. Amith
7635 Plantation Road
1 Roanoke, VA 24019

Xerox - Electro Optical Systems
ATTN: Mr. R. Gammarino
300 North Halstead Street
1 Pasadena, CA 91107

Oregon State University
ATTN: Dr. P. K. Bhattacharya
Dept of Elect & Comp Engineering
1 Corvallis, OR 97331

Commander
US Army CORADCOM
Fort Monmouth, NJ 07703

1 ATTN: DRDCO-COM-RM-1 (Dr. L. Dworkin)
1 DRDCO-COM-RM-1 (Mr. L. Coryell)
9 DRDCO-COM-RM-1 (Ms. C. Loscoe)